

*This contribution is part of the special series of Inaugural Articles by members of the National Academy of Sciences elected on April 28, 1998.*

## Vortices in rotating superfluid $^3\text{He}$

OLLI V. LOUNASMAA\* AND ERKKI THUNEBERG

Low Temperature Laboratory, Helsinki University of Technology, Box 2200, 02015 HUT, Espoo, Finland

Contributed by Olli V. Lounasmaa, April 26, 1999

**ABSTRACT** In this review we first present an introduction to  $^3\text{He}$  and to the ROTA collaboration under which most of the knowledge on vortices in superfluid  $^3\text{He}$  has been obtained. In the physics part, we start from the exceptional properties of helium at millikelvin temperatures. The dilemma of rotating superfluids is presented. In  $^4\text{He}$  and in  $^3\text{He-B}$  the problem is solved by nucleating an array of singular vortex lines. Their experimental detection in  $^3\text{He}$  by NMR is described next. The vortex cores in  $^3\text{He-B}$  have two different structures, both of which have spontaneously broken symmetry. A spin-mass vortex has been identified as well. This object is characterized by a flow of spins around the vortex line, in addition to the usual mass current. A great variety of vortices exist in the A phase of  $^3\text{He}$ ; they are either singular or continuous, and their structure can be a line or a sheet or fill the whole liquid. Altogether seven different types of vortices have been detected in  $^3\text{He}$  by NMR. We also describe briefly other experimental methods that have been used by ROTA scientists in studying vortices in  $^3\text{He}$  and some important results thus obtained. Finally, we discuss the possible applications of experiments and theory of  $^3\text{He}$  to particle physics and cosmology. In particular, we report on experiments where superfluid  $^3\text{He-B}$  was heated locally by absorption of single neutrons. The resulting events can be used to test theoretical models of the Big Bang at the beginning of our universe.

On the scale of a small number of atoms, the behavior of matter is determined by quantum mechanics. Most of this physics is not visible in our everyday life. The reason is that macroscopic bodies consist of enormous numbers of atoms and, instead of their individual motions, one sees only the average behavior that obeys classical laws of physics. Fortunately, there are some systems where the quantum world makes itself visible even on a macroscopic scale. One such system is superfluid  $^3\text{He}$  under rotation (1, 2).

The unusual behavior of  $^3\text{He}$  manifests itself at very low temperatures. The liquid enters the superfluid state, which supports topological defects. An example is the quantized vortex line. Such objects are created spontaneously when the container holding the liquid is put into rotation (Fig. 1). Superfluid  $^3\text{He}$  is the host for a multitude of different types of topological defects, such as point singularities, vortex lines, domain walls, and three-dimensional textures. This behavior allows investigations of general principles, such as topological stability and confinement, nucleation of singularities, and interactions between objects of different topologies. These methods are applicable, for example, to the new and rapidly developing fields of unconventional superconductivity and Bose-Einstein condensation of atomic gases. In addition, there are promising analogies to quantum field theory, elementary particle physics, and cosmology (3, 4).

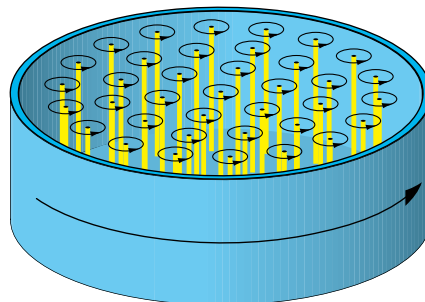


FIG. 1. Rotation of a superfluid is not uniform but takes place via a lattice of quantized vortices, whose cores (yellow) are parallel to the axis of rotation. Small arrows indicate the circulation of the superfluid velocity  $v_s$  around each singularity. The vortex array rotates rigidly with the container. The nearly hexagonal pattern of vortices applies to  $^3\text{He-B}$  and  $^4\text{He}$ .

Superfluid  $^3\text{He}$  shows the most complicated vortex states that exist in nature. Experiments have revealed seven different kinds of vortices in the two superfluid phases,  $^3\text{He-A}$  and  $^3\text{He-B}$  (Fig. 2). Many fascinating properties of the vortex structures have been found. Frequently these are understood in detail because the quasiclassical theory (6) forms a reliable foundation for theoretical studies.

Most of the knowledge on quantum vorticity in  $^3\text{He}$  originates from the Finnish-Soviet ROTA project.<sup>†</sup> These studies have concentrated on identifying the topology and structure of the different objects in the rotating superfluid  $^3\text{He}$ . Work using the first ROTA machine quickly resulted in the discovery of vortices both in the A and B phases (7–10), which was expected, but the great variety of vortex phenomena was a big surprise.

The  $^3\text{He}$  liquid has been investigated typically in a cylindrical container, 7 mm long and 5 mm in diameter, which was rotated

Abbreviations: SMV, spin-mass vortex; SV, singular vortex; LV, locked vortex; VS, vortex sheet; CUV, continuous unlocked vortex.

\*To whom reprint requests should be addressed. e-mail: olli.lounasmaa@hut.fi.

<sup>†</sup>The ROTA collaboration was started in 1978, at the initiative of E.L. Andronikashvili, P.L. Kapitsa, and O.V.L., to investigate the  $^3\text{He}$  superfluids in rotation. The ROTA1 cryostat for this work was completed in Helsinki in 1981 and for ROTA2 in 1988. Over the years, many Russian and Georgian physicists from the Kapitsa and Landau institutes of Moscow and the Andronikashvili Institute of Physics in Tbilisi have worked in Helsinki, together with their Finnish colleagues. The ROTA project was led in 1978–82 by Seppo Islander and since 1983, most of the time, by Matti Krusius. Other group leaders have been Peter Berglund (cryogenics), Pertti Hakonen (NMR and optics), Jukka Pekola (gyroscopy, ultrasonics, and optics), Martti Salomaa (theory), Juha Simola (ion mobility), and E.T. (theory). Theoretical research by Grigori Volovik has been instrumental to the project. Until 1991, ROTA was coordinated by O.V.L. and since then by Matti Krusius. So far the project has produced 20 Ph.D. theses.

around its axis up to 3 rad/s. To study the superfluid state, the liquid must be cooled to a temperature of a few mK and even below. One of the important reasons for the experimental success of the ROTA project has been the combination of dilution refrigeration and adiabatic nuclear demagnetization pioneered in Helsinki (11). The two ROTA cryostats, which contain many innovations in cryogenics and instrumentation, are described in detail in refs. 12 and 13, respectively.

In addition to Helsinki, rotating cryostats for investigations of superfluid  $^3\text{He}$  have been used in three other laboratories. At the University of Manchester, under the leadership of Henry Hall and John Hook, an extensive series of mutual friction experiments have been performed on  $^3\text{He-A}$  and  $^3\text{He-B}$  (14); this work also verified the Helsinki discovery of the vortex core transition in the B phase. At Cornell University, John Reppy's group has investigated persistent currents in  $^3\text{He-A}$  and  $^3\text{He-B}$  by means of the gyroscopic technique (15, 16). At the University of California in Berkeley, Richard Packard's team has measured the circulation of superfluid  $^3\text{He-B}$  by using a vibrating wire (17). The important Berkeley, Cornell, and Manchester experiments on rotating superfluid  $^3\text{He}$  are not discussed here.

The present review is a short semipopular description of the ROTA work. More extensive articles have been published elsewhere (3, 18–23); another ROTA review is under preparation (24).

Plenty of research has been carried out on superfluid  $^4\text{He}$  in rotation (1). This fundamentally important work has been going on for 50 years.

### Superfluids in Rotation

Usually all materials transform into the solid state when temperature is lowered sufficiently. There are two exceptional substances that remain liquid even at the absolute zero. These are the isotopes of helium:  $^3\text{He}$  and  $^4\text{He}$ . Both liquids exhibit very unusual behavior at low temperatures. In particular, they are superfluids,  $^4\text{He}$  below the  $\lambda$  point at 2.2 K and  $^3\text{He}$  below 2.5 mK. Superfluidity is analogous to but not the same phenomenon as superconductivity observed in several metals at low temperatures. In superconductivity the electrical resistivity of the metal disappears; in superfluidity the liquid can flow through narrow tubes without friction.

A superfluid (1, 2) can be thought of as a liquid of two interpenetrating components. The normal fraction behaves like an ordinary liquid whereas the superfluid fraction gives rise to the dissipationless mass flow. These two components

can have different velocities:  $v_n$  for the normal and  $v_s$  for the superfluid fraction.

Although vanishing of the flow resistance is a spectacular phenomenon, the most fundamental property of superfluidity is probed in a different experiment. Let us consider a cylinder holding liquid in the superfluid state. When the container rotates at a constant angular velocity  $\Omega$ , the normal component circulates with the confining vessel similarly to a rigid body. This motion implies that the linear velocity  $v_n = \Omega \times r$  and the vorticity  $\nabla \times v_n = 2\Omega$ ; here  $r$  is the position vector with its origin on the axis of the cylinder.

According to quantum mechanics, all information about a particle is contained in its complex-valued wave function  $\Psi(\mathbf{r}) = |\Psi(\mathbf{r})| \exp[i\Phi(\mathbf{r})]$ . Its velocity is  $\mathbf{v} = (\hbar/m)\nabla\Phi(\mathbf{r})$ , where  $m$  is the mass. The condition  $\nabla \times \mathbf{v} = 0$  then follows because the curl of a gradient is identically zero. This argument applies to all uncharged particles. However, it does not prevent uniform rotation of normal substances because each particle has its own velocity, and these mimic uniform rotation on a scale that is larger than the separation between particles.

Superfluids are different. They are characterized by a macroscopic wave function, i.e., all atoms in the superfluid fraction occupy the same quantum state. These particles have the same velocity  $v_s$  and thus the relationship  $\nabla \times v_s = 0$  is valid even on a macroscopic scale. Therefore, a superfluid cannot rotate like a normal liquid, i.e.,  $v_s \neq v_n$ . In fact, the superfluid remains stationary,  $v_s = 0$ , at small  $\Omega$ , which is called the Landau state.

But a stationary liquid in a rotating container implies a high free energy. When  $\Omega$  increases, the Landau state becomes unstable toward a state having vortex lines (see Fig. 1). The vortex array has been seen directly in rotating superfluid  $^4\text{He}$  by detecting negative ions trapped by the vortex cores (25, 26).

We define a vortex line by the property that the phase  $\Phi$  changes by  $2\pi$  (or some multiple  $n$  of it) when one goes around the line. This property implies that  $\Phi$  and  $v_s$  are not defined in the vortex core. The bulk superfluid outside remains curl free, but  $v_s \neq 0$ . The superfluid circulates around each vortex line with a velocity that is inversely proportional to the distance from the core; such a velocity field is curl free. On the average, however, the superfluid rotates like a normal liquid,  $\langle v_s \rangle = v_n = \Omega \times r$  in equilibrium. This behavior has been verified by measuring the profile of the free liquid surface, both in  $^4\text{He}$  (27) and  $^3\text{He-B}$  (28).

One can define the quantized circulation of the superfluid velocity by  $\kappa = \oint \mathbf{dr} \cdot \mathbf{v}_s$ . Around one vortex line  $\kappa$  equals the circulation quantum,  $\kappa_0 = h/m$ . In  $^3\text{He}$  the relevant mass is twice the atomic mass,  $2m_3$  (see below), and thus  $\kappa_0 = h/2m_3 = 0.066 \text{ mm}^2/\text{s}$ . This value has been verified experimentally within a few percent (17);  $\kappa_0$  is a quantum mechanical constant but, owing to superfluid coherence, it is observable on a macroscopic scale.

The equilibrium number  $N$  of vortices in a rotating container can be deduced from the condition that the circulations of  $v_s$  and  $v_n$  are equal:  $\oint \mathbf{dr} \cdot \mathbf{v}_s = \oint \mathbf{dr} \cdot \mathbf{v}_n$ . Evaluating both sides for a cylindrical container of radius  $R$  gives  $N = 2\pi R^2 \Omega / \kappa_0$ . Thus, there are approximately 600 vortex lines for  $R = 2.5 \text{ mm}$  and  $\Omega = 1 \text{ rad/s}$ .

The discussion above applies to vortices in  $^4\text{He}$  and  $^3\text{He-B}$ . In the case of  $^3\text{He-A}$  some modifications are needed, as will be discussed below. We also note that the flux lines, which occur when type II superconducting metals are placed in a magnetic field, are analogous to vortex lines in superfluids.

In  $^3\text{He}$ , superfluidity can be understood as pairing of atoms, which is analogous to pairing of conduction electrons in superconductors. These Cooper pairs all are in the same pair state, and thus form a macroscopic wave function. The pairing in  $^3\text{He}$  can take place in all three spin triplet states. Likewise, three  $p$ -wave states are available for the orbital part of the wave function. The projection of the macroscopic wave function to

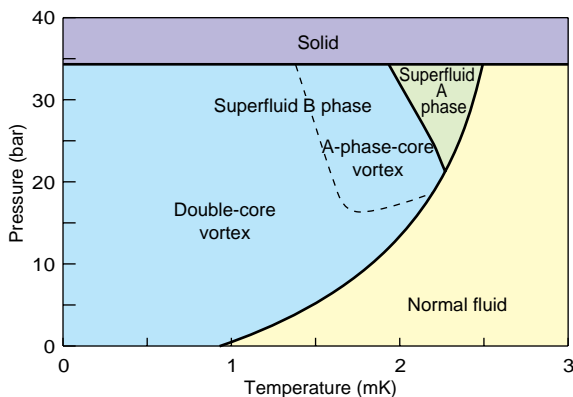


FIG. 2. Phase diagram of  $^3\text{He}$  below 3 mK. The solid phase appears only above the pressure of 34 bar. At high temperatures the liquid is in the normal Fermi state. There are two superfluid phases, A and B. The transition line between the two types of vortex cores in rotating  $^3\text{He-B}$  is shown by the dashed curve. Figure modified from ref. 5.

these states is represented by an order parameter  $A_{ij}$ , which is a complex  $3 \times 3$  matrix. It means that instead of one wave function as in  $^4\text{He}$  one has to deal with a set of nine wave functions in  $^3\text{He}$ , which is the underlying reason for the existence of two superfluid phases, A and B (see Fig. 2). Moreover, it makes different types of vortices possible (see Table 1).

Experimentally it is fortunate that the  $^3\text{He}$  nucleus has a magnetic moment, so that it can be investigated, in contrast to  $^4\text{He}$ , by NMR (40). In this technique, the nuclear moments are excited by a radio-frequency field to precess around a static magnetic field  $H$  at the Larmor frequency  $\nu_L = 32 \text{ MHz} \cdot H/\text{Tesla}$ . In addition, there is a relatively weak dipole-dipole interaction between the nuclei that shifts the frequency upwards from the Larmor value (41). The shifts are different in the A and B phases and depend on the texture of the order parameter  $A_{ij}$ , which allows extraction of information about the number and structure of vortices in both phases.

Most of the experimental ROTA work has been done by using NMR (see below). Other techniques used in Helsinki to study vortices are described only briefly.

### Superfluid $^3\text{He-B}$

NMR experiments on superfluid  $^3\text{He}$  are conducted as follows. First, the  $^3\text{He}$  sample is cooled to the superfluid state around 2 mK. Rotation then is started by slowly accelerating the cryostat from rest. The normal component is viscously coupled to the walls of the container and, at sufficiently slow accelerations, it will rotate uniformly with the container. In contrast, the slippery superfluid fraction remains initially at rest (42, 43), which gives rise to a counterflow,  $v_n - v_s$ , between the normal and superfluid components.

When a critical counterflow velocity, about 5 mm/s in  $^3\text{He-B}$ , is reached, the first vortex is nucleated at the side wall of the container. This singularity is pulled by the Magnus force to the center of the experimental cell. Simultaneously, the circulation drops by an amount equivalent to one circulation quantum  $\kappa_0$ . As the speed of rotation is increased, a second vortex is created when the critical counterflow velocity is reached again. The birth of individual vortices can be observed as jumps in the NMR signal (see Fig. 3). Therefore, during continuous acceleration, quantized vortex lines are accumulated, one by one, to the central region of the container.

NMR spectra measured in  $^3\text{He-B}$  are shown in Fig. 4 (44). In the nonrotating state, the NMR absorption is concentrated to the Larmor frequency (Fig. 4, blue curve). In the rotating state but in the absence of vortices, the Larmor signal decreases and a new counterflow peak is formed at higher frequencies (Fig. 4, red). This peak is reduced when vortices are nucleated (Fig. 4, green). With the equilibrium number of

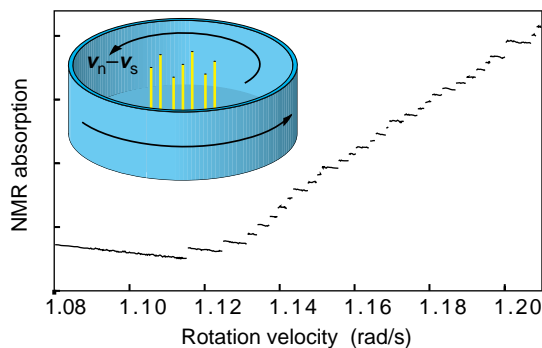


FIG. 3. NMR absorption near the Larmor frequency during acceleration showing the nucleation of single vortex lines, except the third last step that corresponds to two vortices. (Inset) A schematic illustration of a state with less than the equilibrium number of vortex lines. The singularities form a bundle in the center and are surrounded by a vortex-free counterflow region. Figure modified from ref. 44.

vortices, the counterflow is reduced to a minimum and the spectrum is qualitatively similar to that observed at rest.

A change in the NMR absorption was detected in  $^3\text{He-B}$  under rotation (9, 10). This transition arises from a change in the vortex cores. The two structures have been identified by numerical calculations using the Ginzburg-Landau theory of  $^3\text{He}$ . On the low-temperature side of the phase separation curve (dashed line in Fig. 2), vortices have a double core (30) whereas on the high-temperature side the order parameter in the core is similar to that of the bulk A phase (29). Both structures are depicted in Fig. 5. This is an example of a first-order phase transition in a quantized topological object.

Both vortex cores have spontaneously broken symmetry in the order parameter  $A_{ij}$ . The high-temperature vortex is symmetric in rotations around the vortex axis. Broken parity allows the A-phase-like order parameter in the core, which shows up as a bump. In addition to parity, the circular symmetry is broken in the double-core vortex. In this case the core consists of two half-quantum vortices, which manifest themselves as depressions in the order parameter. The half-quantum vortices are bound to each other and cannot be separated more than approximately  $1 \mu\text{m}$ . The broken circular symmetry of the low-temperature vortex was experimentally verified by observing a twist between the two halves of the core (46). Both vortex structures are magnetic, which also has been observed (10).

The underlying reason for the vortex-core transition in  $^3\text{He-B}$  is the multicomponent wave function. In  $^4\text{He}$ , the order parameter is a scalar that has to vanish at the vortex line,  $|\Psi(r)| = 0$ . In  $^3\text{He-B}$ , some components of the wave function must go to zero as well but not all nine components simultaneously.

Table 1. Vortex structures in  $^3\text{He-B}$  and  $^3\text{He-A}$

| Phase           | Vortex type         | $n$ | Lattice | Exper., reference | Theory, reference |
|-----------------|---------------------|-----|---------|-------------------|-------------------|
| $^3\text{He-B}$ | A-phase-core vortex | 1   | hex     | (9, 10)           | (29)              |
|                 | Double-core vortex  | 1   | cr      | (9, 10)           | (30)              |
|                 | SMV                 | 1   | —       | (31)              | (32)              |
| $^3\text{He-A}$ | LV1                 | 4   | sq      | (33)              | (34)              |
|                 | CUV                 | 2   | cr      | (8)               | (35)              |
|                 | SV                  | 1   | cr      | (36)              | (35)              |
|                 | VS                  | 4   | pr      | (37)              | (37)              |
|                 | LV2                 | 2   | cr      | —                 | (38)              |
|                 | LV3                 | 4   | pr      | —                 | (39)              |

The table lists vortex structures that are observed experimentally and/or predicted theoretically in bulk  $^3\text{He}$ . The quantized circulation,  $n\kappa_0$ , refers to one elementary cell. The types (39) of the two-dimensional equilibrium vortex lattices are: hexagonal (hex), square (sq), centered rectangular (cr), and primitive rectangular (pr).

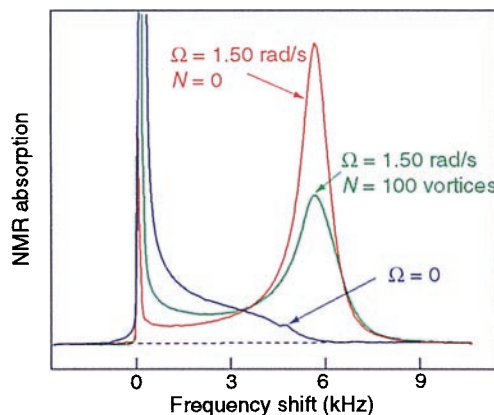


FIG. 4. NMR absorption spectra measured in rotating superfluid  $^3\text{He-B}$ . See text for details. Figure reproduced with permission from ref. 44.

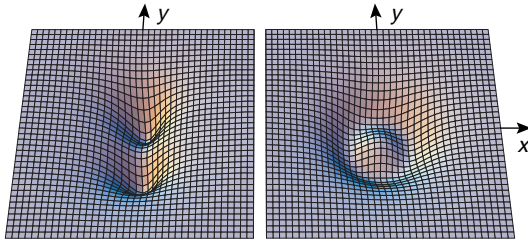


FIG. 5. Magnitude of the order parameter,  $\Sigma_i = 1,2,3 \Sigma_j = 1,2,3 |A_{ij}|^2$  in the two types of vortex cores of  $^3\text{He-B}$ : double-core vortex (Left) and A-phase-core vortex (Right). The magnitude is normalized to unity in bulk  $^3\text{He-B}$  and has a minimum value of 0.5 in the two cores of the double-core vortex. The  $xy$ -plane is perpendicular to the axis of rotation. Vorticity is concentrated into regions where the order parameter is suppressed. The dimensions of the areas shown are on the order of  $1 \mu\text{m}$ . Figure based on calculations in ref. 45.

Therefore, the order parameter is nonzero everywhere in  $^3\text{He-B}$ .

There is also a third kind of vortex in  $^3\text{He-B}$  (31, 47): the spin-mass vortex (SMV). In contrast to the previous two types, this singularity does not form a vortex lattice but appears as a metastable state among usual vortices, as depicted in Fig. 6. The SMV displays, in addition to circulation in the mass flow velocity  $v_s$ , a nonzero circulation in the velocity of the spin flow. In this case particles with opposite spins move in opposite directions. However, the spin is not a strictly conserved quantity, in contrast to mass, which means that the spin flow around an SMV has a range of only  $10 \mu\text{m}$ . Over longer distances the spin flow is concentrated to a planar soliton, which is a domain-wall-like object, attached to the SMV. Consequently, SMVs can appear in two configurations (see Fig. 6): the soliton tail either joins two SMVs to a composite two-quantum vortex, or the SMV is connected to the wall. The dependence of the latter type of soliton on the counterflow velocity has been determined from NMR data (47).

One of the interesting properties to study in  $^3\text{He-B}$  is the nucleation of singular vortices (44). This process involves an energy barrier, similar to that in a first-order phase transition. Because the barrier is relatively high, thermal fluctuations are of minor significance, which means that the barrier effectively has to disappear before the critical velocity  $v_c$  is reached. The measured values of  $v_c$  are roughly one-third of that predicted theoretically for ideally smooth walls. This difference probably originates from imperfections on the container walls.

### Superfluid $^3\text{He-A}$

The order parameter  $A_{ij}$  of the A phase depends on  $\Phi$  and two unit vectors,  $l$  and  $d$ . Here  $l$  gives the direction of the angular momentum of the Cooper pair, while  $d$  determines the orientation of the spin wave function. The relatively weak dipole-

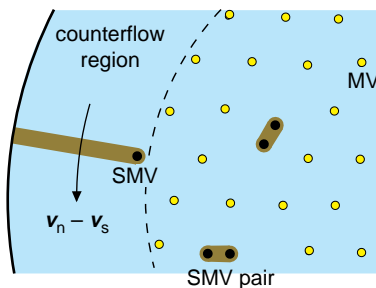


FIG. 6. SMVs in two different configurations. The yellow dots represent usual vortices that have only circulation of mass current (MV). The black dots are SMVs that are tied to a soliton tail (brown). Figure adapted from ref. 31.

dipole interaction tends to align  $l$  and  $d$  parallel or antiparallel to each other (41).

$^3\text{He-A}$  is a very exceptional superfluid because curl  $v_s$  can be nonzero. In spite of this, homogeneous rotation is not possible. The reason is that  $\nabla \times v_s \neq 0$  always implies an inhomogeneous texture of  $l$ . Thus there are two basic types of vortices in the A phase: singular and continuous. Singular vortices are similar to those discussed above in the sense that  $v_s$  is undefined in the core. In continuous vorticity,  $v_s$  is defined everywhere and, as a consequence,  $\nabla \times v_s \neq 0$  arises from the texture of  $l$ .

Different kinds of vortices that are present in  $^3\text{He-A}$  are depicted in Fig. 7 (48). The arrows denote the  $l$ -vectors on the  $xy$ -plane, which is perpendicular to the axis of rotation. There is only one singular vortex (SV). Its “hard” core, where  $v_s$  is undefined, has a diameter on the order of the superfluid coherence length  $\xi = 10\text{--}100 \text{ nm}$ . Inside the hard core the order parameter deviates strongly from its form in the bulk liquid. In addition, the SV has a “soft” core where  $l \neq d$ .

All other structures depicted in Fig. 7 are continuous and thus do not have a hard core. The yellow shading marks regions where  $\nabla \times v_s \neq 0$  because of the  $l$ -texture. These regions have different dimensions: the locked vortex 1 (LV1) fills the whole space, the vortex sheet (VS), and the LV 3 (LV3) form two-dimensional sheets, and the continuous unlocked vortex (CUV) and the SV have a line structure. More precisely, the vorticity in the CUV is concentrated in a cylindrical region because vorticity on the axis is small; the CUV can be interpreted as a VS that is closed to a cylinder.

There is a fundamental theorem (49) that relates the texture of  $l$  to the circulation of the superfluid,  $\kappa = n\kappa_0$ . It says that if  $l$  goes through all directions on a unit sphere, then the circulation around such object corresponds to two quanta, i.e.,  $n = 2$ . It can be seen from Fig. 7 that  $l$  sweeps once the unit sphere for the VS, CUV, and LV3. Therefore, all these have the circulation of two quanta. In the LV1,  $l$  sweeps the unit sphere twice, and thus this vortex has four quanta,  $n = 4$ . The theorem holds strictly for continuous vortices only, but it can be applied also to the SV, where  $l$  covers approximately half of the unit sphere and  $n = 1$ . Somewhat surprisingly, the contribution of the hard core to the circulation is very small in the SV.

The relative stability of the different vortices is not affected much by temperature or pressure, but depends crucially on the rotation velocity  $\Omega$  and on the magnetic field  $H$ . Continuous vortices, in which  $l$  and  $d$  follow each other, are called locked, whereas structures with a soft core, where the directions of the unit vectors  $l$  and  $d$  differ substantially, are unlocked. The dipole-dipole interaction favors locked structures. The field tries to keep  $d$  perpendicular to  $H$ , which makes unlocked structures (VS, CUV, and SV) preferred in high fields (see Fig. 7). The SV is energetically favorable at a slow rotation velocity because it has the lowest circulation quantum number,  $n = 1$ .

The phase diagram can be measured by cooling the  $^3\text{He}$  sample slowly through the superfluid transition while continuously rotating the cryostat. The experiments cannot yet distinguish between different types of locked vortices (see Table 1). The calculated diagram of Fig. 7 is in semiquantitative agreement with experiments (39, 48).

Different NMR absorption spectra for  $^3\text{He-A}$  are illustrated in Fig. 8 (50). In all cases, the large main peak is shifted toward higher frequencies by about 15 kHz from the Larmor value. The satellite peaks on the low-frequency side are caused by the presence of vortices. They correspond to spin-wave modes localized in the soft cores, which is associated with oscillations of  $d$ .

The doubly quantized CUV (see Fig. 7) has a singularity-free soft core that is twice larger than the soft core of the SV. Depending on the size and structure of the soft core, oscillations take place at different frequencies, which makes it possible to distinguish between the structures. The differences

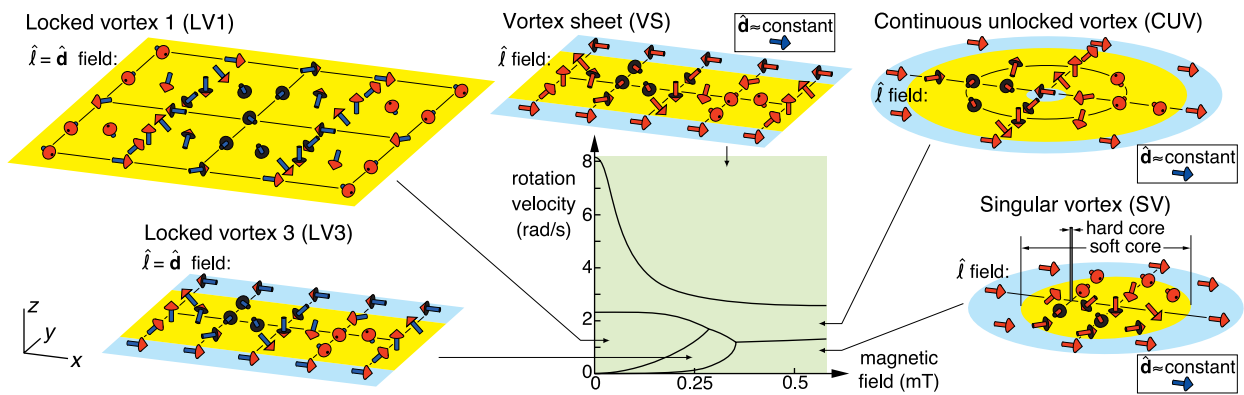


FIG. 7. Different types of  $l$ -textures in rotating superfluid  $^3\text{He-A}$ . The phase diagram in the  $\Omega$  vs.  $H$ -plane is shown in the middle. The yellow shading denotes regions with vorticity,  $\nabla \times \mathbf{v}_s \neq 0$ . In the blue areas outside,  $\text{curl } \mathbf{v}_s = 0$ . Only half of the elementary cell is shown for VS and LV3. For more details, see text. Figure adapted from ref. 48.

in the NMR satellite frequencies and in the intensities of the CUV and SV peaks are largely the result of the smaller soft core of the latter.

Besides vortices, other defects can appear in  $^3\text{He-A}$  as well. Fig. 8 shows, as examples, the spectra in the presence of splay and twist solitons, which are planar, domain-wall-like objects that separate two regimes having parallel and antiparallel orientations of  $l$  and  $d$ , respectively. Solitons sometimes appear when a  $^3\text{He}$  sample is cooled rapidly into the superfluid state, and they may remain trapped in the experimental cell for a long time.

The VS was discovered in  $^3\text{He-A}$  in 1993 (37). The concept is an old one. Cylindrical VSs were proposed by Onsager (51) and by Fritz London (52) in the late forties and early fifties as the first attempt to explain the mysterious flow properties of  $^4\text{He}$ , the only superfluid known at that time. The model was further developed by Landau and Lifshitz (53), who calculated the separation between the vortex cylinders. In the  $^4\text{He}$  superfluid, however, the VS is unstable and breaks into separate vortex lines.

In  $^3\text{He-A}$  the VS is stable (22, 54). Its macroscopic structure in a rotating container is illustrated in Fig. 9. The backbone of the sheet is a two-dimensional soliton. Suppose a vertical soliton wall is present initially in a stationary container. When rotation is started, it is easier to form vortex quanta within the existing soliton than to nucleate separate vortex lines, which involves a higher energy barrier. In this way continuous vorticity is added to the soliton, which develops into a VS and grows with increasing rotation velocity because vortices repel each other if their density is high. This repulsion leads to folding of the VS shown in the upper part of Fig. 9. The number of convolutions increases with the speed of rotation; at  $\Omega = 1$  rad/s, the distance between the folds is  $350 \mu\text{m}$ , 10 times more than the thickness of the sheet.

$^3\text{He-A}$  is also exceptional in the nucleation of vortices. In the more usual superfluids, vortices are created at the walls of the container because the counterflow is largest there. Moreover, the unavoidable roughness of real container walls always lowers the threshold for nucleation. Therefore, the intrinsic critical velocity of the bulk superfluid is not easily accessible to experiments.  $^3\text{He-A}$  is an exception to this rule because the critical velocity is determined by nucleation of continuous

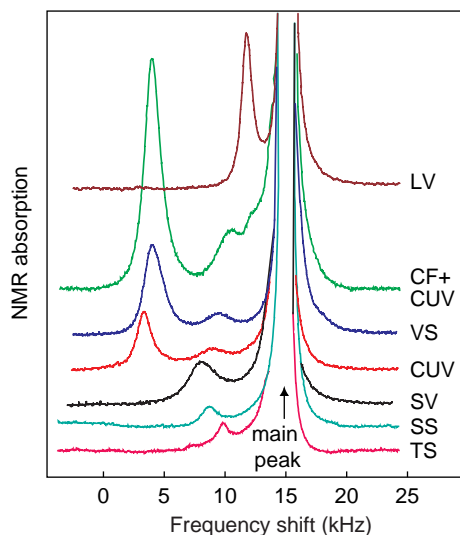


FIG. 8. NMR absorption spectra of different topological objects in rotating  $^3\text{He-A}$ . In each case the main peak arises from the bulk liquid. Every defect (vortex or soliton) gives rise to a satellite peak at a characteristic frequency. The heights of the satellites are directly proportional to the number of each type of defect in the experimental cell. Compare with Fig. 7 and Table 1. For clarity the different spectra are shifted vertically. CF, counterflow region; SS, splay soliton; TS, twist soliton. Figure reproduced with permission from ref. 50.

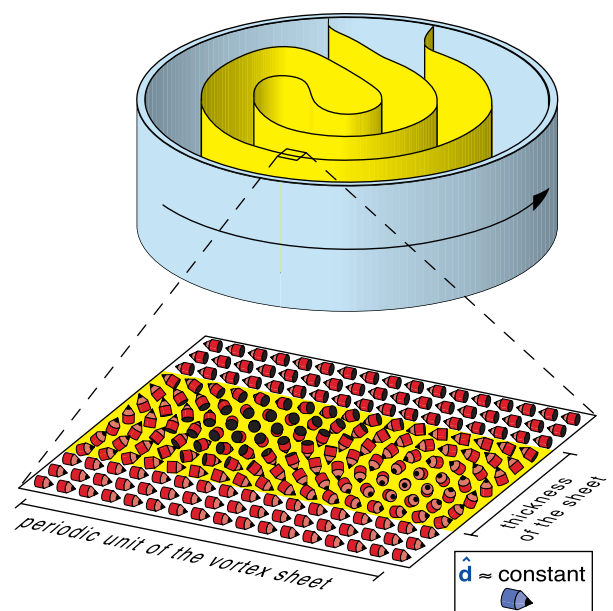


FIG. 9. Folding of the VS in a rotating container (Upper) and one periodic unit of the  $l$ -vector field associated with it (Lower). In the VS  $l$  is unlocked from  $d$ , which is pointing toward right, perpendicular to  $H$ . Figure adapted from ref. 55.

vorticity. There  $l$  is fixed perpendicular to the walls, and the  $l$ -field can be bent only at a distance larger than the dipole coherence length  $\xi_D \approx 10 \mu\text{m}$  from a wall. Thus the formation of continuous vorticity is a process in the bulk liquid, generally beyond the reach of surface roughness (56).

The stability of the bulk flow can be accurately studied theoretically. In a certain range of parameters, a transition to a helical  $l$ -texture is found. Measurements show some scatter of the critical velocity because  $v_c$  also depends on the overall  $l$ -texture in the experimental cell. Anyway, the agreement between theoretically calculated and measured critical velocities is better in  $^3\text{He-A}$  than in any other superfluid (56).

Most of the vortex structures in  $^3\text{He-A}$  remain metastable even though they do not correspond to the minimum of energy, which means that it is possible to create rotating states where different types of vortices are present together (57). In particular, the coexistence of single- and double-quantum vortex lines can be investigated.

The A and B phases also may be simultaneously present in a rotating container. Because the two are phase coherent, vortices cannot terminate at the A-B interface but must continue through or align with the boundary. However, the textures are very different on both sides, so a severe adjustment has to take place at the interface. Experiments show that in the case of a slowly moving boundary, the A-phase vortices are pushed away in front of the interface, and penetration takes place only at faster rates of transition (58, 59).

### Studies Using Gyroscopy, Ion Mobility, Ultrasonics, and Optical Techniques

The experimental ROTA work described so far is based on sensitive NMR measurements. Important results on rotating superfluid  $^3\text{He}$  have been obtained by using other techniques as well.

Gyroscopy was first used on  $^3\text{He}$  by John Reppy's group at Cornell (15, 16) and then in Helsinki (5, 60, 61) for persistent current measurements in a toroidal ring. When the ring was driven about one of its major axes at the resonant frequency of the perpendicular axis, a sinusoidal response resulted, provided that there was angular momentum  $L$  in the ring, caused by the circulating superfluid.

A careful check for possible weak dissipation was made in  $^3\text{He-B}$  (60). After having kept the liquid in the B phase continuously for 48 h, the angular momentum in the ring was measured. Within the experimental accuracy of 10% in the  $L$  data, there had been no decay of the signal. This observation yields a relaxation time of the superflow in excess of 450 h and implies a viscosity that is at least 12 orders of magnitude lower than for the normal Fermi liquid at the same temperature.  $^3\text{He-B}$  thus seems to be a true superfluid.

Ion mobility is one of the observables that can be used, in addition to NMR, for probing the soft vortex cores (62). An ion, which is a 1-nm "bubble" containing an electron, moves in an electric field with the drift velocity  $v_d$  and interacts with the  $l$ -texture of the soft vortex cores. The ion mobility is at its maximum when the  $l$ -vector is perpendicular to  $v_d$ . Textures typical in the vicinity of vortices give rise to focusing of ion trajectories.

Two different rotating states have been discovered by using negative ions in  $^3\text{He-A}$  (36, 63): regime a, resulting from a rapid 30-s speed-up of the cryostat, and regime b, created by a long stepwise acceleration. In regime a, a clear slowing down of the ions was observed, accompanied by a prominent change in the shape of the collected current pulses, whereas in regime b there was no change. The texture in the latter case was interpreted as a focusing SV structure with a large mobility along its cores, which was the first evidence of SVs (Fig. 7) in rotating  $^3\text{He-A}$  (36). Later they were seen in NMR experiments as well (48).

Ultrasonics has been used to study vortices in  $^3\text{He-A}$  (33, 64). The attenuation of zero sound in the A phase is larger when  $l$  is parallel to the propagation of sound compared with the perpendicular case. Therefore, it is possible to distinguish, for example, between LV1 and CUV (see Table 1). In the former texture, all directions of  $l$  are nearly equally present whereas in the latter  $l$  is constant except inside the soft core (see Fig. 7), which occupies only a small fraction of the total volume at the experimental rotation velocities  $\Omega < 3 \text{ rad/s}$ . When a sound pulse is transmitted parallel to  $\Omega$ , the attenuation should be larger for LV1. Experimentally two states were found, the one present in a lower magnetic field having larger attenuation. This observation is consistent with the phase diagram of Fig. 7.

Optical studies were extended for the first time by one of the ROTA groups into the superfluid phases of  $^3\text{He}$  (28). The rather advanced technique (65, 66) involved analysis of circular interference rings generated by a parallel beam of laser light and reflected from the liquid surface and from the bottom of the optical cell.

The free meniscus of the rotating liquid acted as a parabolic mirror. Both in the normal Fermi liquid and the superfluid phases the  $\Omega$ -dependent focal lengths were equal. This result shows that the superfluid surface had the same parabolic shape as the surface of the normal liquid, indicating that the equilibrium number of vortices was present in  $^3\text{He-B}$ . At low rotation speeds, clear evidence for Landau's vortex-free state was obtained.

### Superfluid $^3\text{He}$ in Cosmology

The topological objects in the order parameter field of superfluid  $^3\text{He}$ , such as textural point defects, quantized vortex lines, and solitons, are in many respects similar to monopoles, strings, and domain walls in relativistic quantum field theories (3, 4, 23, 24). In high-energy physics these objects are still hypothetical, whereas in the case of superfluid  $^3\text{He}$  they can be observed experimentally. Here we discuss just one example: an experiment modeling developments in the early universe. The study (67, 68) involves creation of vortices by absorption of neutrons in rotating superfluid  $^3\text{He-B}$ .

The mass in the universe is very unevenly distributed. There are galaxies and clusters of them, even clusters of clusters, while large regions of the universe appear to be devoid of any visible mass. This inhomogeneity somehow must have started after the universe was created in the Big Bang about 15 billion years ago. A large-scale anisotropy recently also has been detected in the 2.7-K cosmic background radiation, which originates from the time 300,000 years after the Big Bang.

According to the theories proposed by Kibble (69) and Zurek (70), the reasons for this uneven distribution of matter and radiation are the rapid phase transitions, which created topological defects, such as massive cosmic strings, after the Big Bang. The theory is capable of explaining the uneven distribution of mass in the present universe. Topological defects were formed in symmetry-breaking phase transitions when the temperature dropped below a critical value.

Fig. 10 explains the experiment performed in Helsinki (67). Superfluid  $^3\text{He-B}$  was rotated below the critical velocity limit in a 5-mm diameter cylinder at  $T \approx 1 \text{ mK}$ , so that vortices were not created until a paraffin-moderated Am-Be neutron source was brought close to the sample (Fig. 10a). For thermal neutrons the mean free path is 0.1 mm in liquid  $^3\text{He}$  so that the absorption reactions occur close to the walls of the sample container. When a  $^3\text{He}$  nucleus absorbs a neutron, a "Mini Bang" occurs,  $n + ^3\text{He} \rightarrow p + ^3\text{H} + 764 \text{ keV}$ . The nucleus thus splits to a proton and a triton, which fly in opposite directions, producing 70- $\mu\text{m}$  and 10- $\mu\text{m}$  long ionization tracks, respectively (Fig. 10b). The subsequent charge recombination yields a 0.1-mm long cigar-shaped region of normal  $^3\text{He}$  (Fig. 10c).

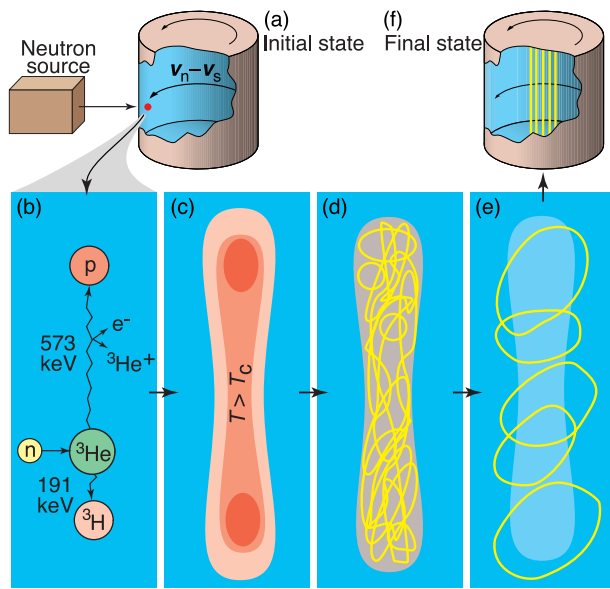


FIG. 10. Schematic illustration and interpretation of the Mini Bang experiment. See text for details. Figure modified from ref. 67.

The heated volume cools so fast back to the superfluid state that relaxation of the order parameter lags behind and the equilibrium state cannot be established. According to the theories of Kibble (69) and Zurek (70), vortices are created during this transition (Fig. 10d).

A special feature of the Helsinki experiment is the applied bias flow caused by rotation, which forces the larger vortex loops to expand instead of shrink (Fig. 10e). They hit the walls and straighten to rectilinear vortex lines in the center of the cylinder (Fig. 10f). The formation of vortices could be verified experimentally as distinct steps, in the same way as in Fig. 3. By varying the parameters it was established that the measurements agreed with the predicted distribution of the loop sizes. Evidence of competing A- and B-phase regions also was found (68).

In a related experiment (71) at Grenoble, in collaboration with George Pickett's group of Lancaster University, a calorimetric technique was used at the record-low temperature of 130  $\mu$ K. The vortex loops decay very slowly in such extreme cold. They could not be observed directly, but their density was inferred from the amount of energy that was not detected as heat.

The relaxation of energy from 764 keV to the level of 0.1 eV for each vortex ring is a complicated process, and many details are still unknown. The experimental indications are consistent with the theories proposed by Kibble (69) and Zurek (70), and further applied by Kibble and Volovik (24). Nevertheless, the Kibble-Zurek mechanism recently has become the subject of debates among condensed matter physicists. However, if the theory can be verified in  $^3\text{He-B}$ , the argument that it also can explain how the inhomogeneity of the universe started soon after the Big Bang would be strengthened.

## Conclusions

When the experimental studies on rotating  $^3\text{He}$  were started in 1978, there were a few predictions of novel vortex structures in  $^3\text{He-A}$ . Over the years experiments have yielded a lot of new and unexpected information about vortices and other topological objects in the A and B phases. In many cases detailed explanations of experimental results are now available. The behavior of these structures has been studied under many different circumstances. For example, nucleation of vortices during increasing counterflow and when the  $^3\text{He}$  sample is

cooling through the superfluid transition, annihilation of vortices, their interactions with surfaces and with the A-B phase boundary, the NMR response of different vortices, and the effect of ultrasound as well as ion mobility have been investigated.

New findings have been made steadily for almost 20 years, and more are expected. For example, there is not yet observation of the half-quantum vortex that is the predicted termination line of the VS in  $^3\text{He-A}$ . New vortex types are expected under different conditions: ultrafast rotation, the zero-temperature limit, high magnetic fields, and restricted geometries. Point defects have not been observed directly yet, but are predicted in the bulk liquid, on container walls, and on the A-B interface.

The study of superfluid  $^3\text{He}$  in rotation is basic research, where the main motivation is to gain information on this fascinating liquid.  $^3\text{He}$  provides a well-understood example, which is valuable for analyzing other systems where theory and/or experiments are less developed. Promising parallels exist in superconductivity, Bose-Einstein-condensed systems, quantum field theory, particle physics, and cosmology. For this work, superfluid  $^3\text{He}$  is an ideal laboratory model, because it is the most complex coherent many-body system available but simultaneously it can be described by the highly successful quasiclassical theory.

Our manuscript was critically read by Pertti Hakonen, Matti Krusius, and Grigori Volovik, who also made suggestions about its contents. We are grateful to our sponsors and advisers. ROTA research has been supported by the Academy of Finland, the Soviet (later Russian) Academy of Sciences, and the Finnish-Soviet Commission for Scientific and Technical Cooperation.

1. Tilley, D. R. & Tilley, J. (1990) *Superfluidity and Superconductivity* (Hilger, Bristol, U.K.).
2. Vollhardt, D. & Wölfle, P. (1990) *The Superfluid Phases of Helium 3* (Taylor & Francis, London).
3. Volovik, G. E. (1992) *Exotic Properties of Superfluid  $^3\text{He}$*  (World Scientific, Singapore).
4. Volovik, G. E. (1999) *Proc. Natl. Acad. Sci. USA* **96**, 6042–6047.
5. Pekola, J. P., Simola, J. T., Hakonen, P. J., Krusius, M., Lounasmaa, O. V., Nummila, K. K., Mamniashvili, G., Packard, R. E. & Volovik, G. E. (1984) *Phys. Rev. Lett.* **53**, 584–587.
6. Serene, J. W. & Rainer, D. (1983) *Phys. Rep.* **101**, 221–311.
7. Hakonen, P. J., Ikkala, O. T., Islander, S. T., Lounasmaa, O. V., Markkula, T. K., Roubeau, P., Saloheimo, K. M., Volovik, G. E., Andronikashvili, E. L., Garibashvili, D. I. & Tsakade, J. S. (1982) *Phys. Rev. Lett.* **48**, 1838–1841.
8. Hakonen, P. J., Ikkala, O. T. & Islander, S. T. (1982) *Phys. Rev. Lett.* **49**, 1258–1261.
9. Ikkala, O. T., Volovik, G. E., Hakonen, P. J., Bunkov, Y. M., Islander, S. T. & Kharadze, G. A. (1982) *JETP Lett.* **35**, 416–420.
10. Hakonen, P. J., Krusius, M., Salomaa, M. M., Simola, J. T., Bunkov, Y. M., Mineev, V. P. & Volovik, G. E. (1983) *Phys. Rev. Lett.* **51**, 1362–1365.
11. Ahonen, A. I., Haikala, M. T., Krusius, M. & Lounasmaa, O. V. (1974) *Phys. Rev. Lett.* **33**, 628–631.
12. Hakonen, P. J., Ikkala, O. T., Islander, S. T., Markkula, T. K., Roubeau, P. M., Saloheimo, K. M., Garibashvili, D. I. & Tsakadze, J. S. (1983) *Cryogenics* **23**, 243–250.
13. Salmelin, R. H., Kyyräräinen, J. M., Berglund, M. P. & Pekola, J. P. (1989) *J. Low Temp. Phys.* **76**, 83–106.
14. Bevan, T. D., Manninen, A. J., Cook, J. B., Alles, H., Hook, J. R. & Hall, H. E. (1997) *J. Low Temp. Phys.* **109**, 423–459.
15. Gammel, P. L., Hall, H. E. & Reppy, J. D. (1984) *Phys. Rev. Lett.* **52**, 121–124.
16. Gammel, P. L., Ho, T.-L. & Reppy, J. D. (1985) *Phys. Rev. Lett.* **55**, 2708–2711.
17. Zieve, R. J., Mukharsky, Y. M., Close, J. D., Davis, J. C. & Packard, R. E. (1993) *J. Low Temp. Phys.* **91**, 315–339.
18. Mineev, V. P., Salomaa, M. M. & Lounasmaa, O. V. (1986) *Nature (London)* **324**, 333–340.
19. Salomaa, M. M. & Volovik, G. E. (1987) *Rev. Mod. Phys.* **59**, 533–613, and erratum (1988), **60**, 573.

20. Hakonen, P., Lounasmaa, O. V. & Simola, J. (1989) *Physica B* **160**, 1–55.
21. Krusius, M. (1993) *J. Low Temp. Phys.* **91**, 233–273.
22. Thuneberg, E. V. (1995) *Physica B* **210**, 287–299.
23. Volovik, G. E. (1998) *Physica B* **255**, 86–107.
24. Eltsov, V. B., Krusius, M. & Volovik, G. E. (1998) e-Print Archive, <http://xxx.lanl.gov/abs/cond-mat/9809125>.
25. Williams, G. A. & Packard, R. E. (1974) *Phys. Rev. Lett.* **33**, 280–283.
26. Yarmchuk, E. J. & Packard, R. E. (1982) *J. Low Temp. Phys.* **46**, 479–515.
27. Osborne, D. V. (1950) *Proc. Phys. Soc. London A* **63**, 909–912.
28. Manninen, A. J., Pekola, J. P., Kira, G. M., Ruutu, J. P., Babkin, A. V., Alles, H. & Lounasmaa, O. V. (1992) *Phys. Rev. Lett.* **69**, 2392–2395.
29. Salomaa, M. M. & Volovik, G. E. (1983) *Phys. Rev. Lett.* **51**, 2040–2043.
30. Thuneberg, E. V. (1986) *Phys. Rev. Lett.* **56**, 359–362.
31. Kondo, Y., Korhonen, J. S., Krusius, M., Dmitriev, V. V., Thuneberg, E. V. & Volovik, G. E. (1992) *Phys. Rev. Lett.* **68**, 3331–3334.
32. Thuneberg, E. V. (1987) *Europhys. Lett.* **3**, 711–715.
33. Pekola, J. P., Toriuka, K., Manninen, A. J., Kynnäräinen, J. M. & Volovik, G. E. (1990) *Phys. Rev. Lett.* **65**, 3293–3296.
34. Fujita, T., Nakahara, M., Ohmi, T. & Tsuneto, T. (1978) *Prog. Theor. Phys.* **60**, 671–682.
35. Seppälä, H. K. & Volovik, G. E. (1983) *J. Low Temp. Phys.* **51**, 279–290.
36. Simola, J. T., Skrbek, L., Nummila, K. K. & Korhonen, J. S. (1987) *Phys. Rev. Lett.* **58**, 904–907.
37. Parts, Ü., Thuneberg, E. V., Volovik, G. E., Koivuniemi, J. H., Ruutu, V. M., Heinilä, M., Karimäki, J. M. & Krusius, M. (1994) *Phys. Rev. Lett.* **72**, 3839–3842.
38. Zotos, X. & Maki, K. (1985) *Phys. Rev. B* **31**, 7120–7123.
39. Karimäki, J. M. & Thuneberg, E. V. (1999) e-Print Archive, <http://xxx.lanl.gov/abs/cond-mat/9902207>.
40. Hakonen, P. J., Ikkala, O. T., Islander, S. T., Lounasmaa, O. V. & Volovik, G. E. (1983) *J. Low Temp. Phys.* **53**, 425–476.
41. Leggett, A. J. (1975) *Rev. Mod. Phys.* **47**, 331–414.
42. Hakonen, P. J. & Nummila, K. K. (1987) *Phys. Rev. Lett.* **59**, 1006–1009.
43. Korhonen, J. S., Gongadze, A. D., Janú, Z., Kondo, Y., Krusius, M., Mukharsky, Y. M. & Thuneberg, E. (1990) *Phys. Rev. Lett.* **65**, 1211–1214.
44. Ruutu, V. M., Parts, Ü., Koivuniemi, J. H., Kopnin, N. B. & Krusius, M. (1997) *J. Low Temp. Phys.* **107**, 93–164.
45. Thuneberg, E. V. (1987) *Phys. Rev. B* **36**, 3583–3597.
46. Kondo, Y., Korhonen, J. S., Krusius, M., Dmitriev, V. V., Mukharsky, Y. M., Sonin, E. B. & Volovik, G. E. (1991) *Phys. Rev. Lett.* **67**, 81–84.
47. Korhonen, J. S., Kondo, Y., Krusius, M., Thuneberg, E. V. & Volovik, G. E. (1993) *Phys. Rev. B* **47**, 8868–8885.
48. Parts, Ü., Karimäki, J. M., Koivuniemi, J. H., Krusius, M., Ruutu, V. M., Thuneberg, E. V. & Volovik, G. E. (1995) *Phys. Rev. Lett.* **75**, 3320–3323.
49. Mermin, N. D. & Ho, T.-L. (1976) *Phys. Rev. Lett.* **36**, 594–597.
50. Ruutu, V. M., Parts, Ü. & Krusius, M. (1996) *J. Low Temp. Phys.* **103**, 331–343.
51. Onsager, L. (1949) *Nuovo Cimento* **6**, Suppl. 2, 249–250.
52. London, F. (1954) *Superfluids* (Dover, New York).
53. Landau, L. D. & Lifshitz, E. M. (1955) *Dokl. Akad. Nauk. SSSR* **100**, 669–672.
54. Parts, Ü., Ruutu, V. M., Koivuniemi, J. H., Krusius, M., Thuneberg, E. V. & Volovik, G. E. (1995) *Physica B* **210**, 311–333.
55. Thuneberg, E. V. (1995) *J. Low Temp. Phys.* **101**, 135–140.
56. Ruutu, V. M., Kopu, J., Krusius, M., Parts, Ü., Plaçais, B., Thuneberg, E. V. & Xu, W. (1997) *Phys. Rev. Lett.* **79**, 5058–5061.
57. Parts, Ü., Avilov, V. V., Koivuniemi, J. H., Kopnin, N. B., Krusius, M., Ruohio, J. J. & Ruutu, V. M. (1999) e-Print Archive, <http://xxx.lanl.gov/abs/cond-mat/9905356>.
58. Parts, Ü., Kondo, Y., Korhonen, J. S., Krusius, M. & Thuneberg, E. V. (1993) *Phys. Rev. Lett.* **71**, 2951–2954.
59. Krusius, M., Thuneberg, E. V. & Parts, Ü. (1994) *Physica B* **197**, 376–389.
60. Pekola, J. P., Simola, J. T., Nummila, K. K., Lounasmaa, O. V. & Packard, R. E. (1984) *Phys. Rev. Lett.* **53**, 70–73.
61. Pekola, J. P. & Simola, J. T. (1985) *J. Low Temp. Phys.* **58**, 555–590.
62. Simola, J. T., Nummila, K. K., Hirai, A., Korhonen, J. S., Schoepe, W. & Skrbek, L. (1986) *Phys. Rev. Lett.* **57**, 1923–1926.
63. Nummila, K. K., Simola, J. T. & Korhonen, J. S. (1989) *J. Low Temp. Phys.* **75**, 111–157.
64. Kynnäräinen, J. M., Pekola, J. P., Torizuka, K., Manninen, A. J. & Babkin, A. V. (1991) *J. Low Temp. Phys.* **82**, 325–367.
65. Alles, H., Ruutu, J. P., Babkin, A. V., Hakonen, P. J., Lounasmaa, O. V. & Sonin, E. B. (1995) *Phys. Rev. Lett.* **74**, 2744–2747.
66. Alles, H., Ruutu, J. P., Babkin, A. V., Hakonen, P. J. & Sonin, E. B. (1996) *J. Low Temp. Phys.* **102**, 411–443.
67. Ruutu, V. M., Eltsov, V. B., Gill, A. J., Kibble, T. W. B., Krusius, M., Makhlin, Y. G., Plaçais, B., Volovik, G. E. & Xu, W. (1996) *Nature (London)* **382**, 334–336.
68. Ruutu, V. M., Eltsov, V. B., Krusius, M., Makhlin, Y. G., Plaçais, B. & Volovik, G. E. (1998) *Phys. Rev. Lett.* **80**, 1465–1468.
69. Kibble, T. V. B. (1976) *J. Phys. A* **9**, 1387–1398.
70. Zurek, W. H. (1985) *Nature (London)* **317**, 505–508.
71. Bäuerle, C., Bunkov, Y. M., Fisher, S. N., Godfrin, H. & Pickett, G. E. (1996) *Nature (London)* **382**, 332–334.